JOURNAL OF GEOPHYSICAL RESEARCH, VOL. 99, NO. C1, PAGES 775–789, JANUARY 15, 1994

Ripple geometry in wave-dominated environments

Patricia L. Wiberg and Courtney K. Harris

Department of Environmental Sciences, University of Virginia, Charlottesville

The wavelength, height, and steepness of ripples formed under oscillatory flows in flume and field studies are reexamined to construct a simple and accurate method of predicting these ripple properties. Ripples with wavelengths proportional to near-bed wave orbital diameter (orbital ripples), predominant in laboratory experiments, are found to have heights in excess of the thickness of the wave boundary layer. Ripples with wavelengths that are roughly proportional to grain size and nearly independent of orbital diameter (anorbital ripples), which predominate in the field, have heights at least several times smaller than wave boundary layer thickness. Relating wave boundary layer height to the generally more easily estimated wave orbital diameter, a set of expressions are developed for predicting ripple type and geometry based on mean grain size, wave orbital diameter, and estimated anorbital ripple height. This method provides a good characterization of ripple wavelength and steepness for a large set of combined field and flume data.

Introduction

The geometry of wave-generated ripples in environments in which surface gravity waves impinge on an erodible bed, e.g., the nearshore zone and much of the continental shelf, is important for bottom boundary layer flow, sediment transport, and wave energy dissipation calculations. As a result, numerous studies have investigated the relationship between wave parameters, grain size, and ripple geometry in laboratory and field settings. Laboratory studies include those of *Bagnold* [1946], *Manohar* [1955], *Yalin and Russell* [1962], *Kennedy and Falcon* [1965], *Horikawa and Watanabe* [1967], *Carstens et al.* [1969], *Mogridge and Kamphuis* [1972], *Dingler* [1974], and *Miller and Komar* [1980a]. These studies have been conducted in a variety of types of flumes and for a large range of sediment sizes and densities. (See summaries by *Miller and Komar* [1980a], *Dingler* [1974], and *Vongvisessomjai* [1984].) One notable limitation to these measurements is the relatively low wave periods used in most cases owing to limitations of the experimental apparatus. Field studies include those of *Inman* [1957], *Dingler* [1974], and *Miller and Komar* [1980b]. Average wave period in these studies is generally longer than in the laboratory studies, but the wave field is typically comprised of a range of wave heights and periods, complicating the interpretation of the relationship between wave conditions and measured ripple geometry.

Analyses of ripple wavelengths, λ, indicate that most wave-formed ripples fall into one of three categories. At small values of the ratio of wave orbital diameter to mean grain diameter, d_o/D, ripple wavelength, or spacing, is proportional to d_o. *Clifton* [1976] refers to these as orbital ripples. At relatively large values of d_o/D, ripple wavelength appears to be a roughly constant multiple of grain size (~500D) and is nearly independent of d_o. *Clifton* [1976] refers to these as anorbital ripples. A transitional range of d_o/D values exists at intermediate wave conditions in which both anorbital and orbital ripples appear possible, as well as ripples having intermediate wavelengths, termed suborbital ripples [*Clifton*, 1976]. In this transitional range of wave conditions, ripple wavelengths measured in the laboratory and field can differ by more than a factor of 3 at a given d_o/D. Conditions on the continental shelf most often fall in the range for suborbital and anorbital ripples, although orbital ripples are occasionally found.

Other important geometric properties of wave-generated ripples are ripple height, η, steepness (ripple height to wavelength ratio, η/λ), and symmetry. Ripple height is more difficult to measure than ripple wavelength and was omitted in some studies. Analyses of ripple steepness indicate that steepness is nearly constant for orbital ripples, with a typical value of 0.17. The steepness of anorbital ripples is significantly smaller and decreases with increasing wave conditions for a given grain size. The decrease in steepness is primarily associated with decreasing ripple height, probably as a result of suspension of sediment at ripple crests. Under purely oscillatory flows, bed ripples tend to be symmetric in cross section, with broad troughs and narrow crests. The superposition of a mean current on an oscillatory flow can add a degree of asymmetry to the ripples in the direction of the mean flow; asymmetry in orbital velocities can also cause ripple asymmetry [*Clifton and Dingler*, 1984]. In this analysis, we focus on symmetric ripples.

Available empirical expressions for predicting ripple wavelength and height (or steepness) for a given flow condition and bed sediment size generally are based on either laboratory data or field data, but rarely both. *Grant and Madsen* [1982] primarily used the *Carstens et al.* [1969] flume measurements of ripple spacing and height to develop general expressions for ripple height and steepness. *Nielsen* [1981] developed two sets of empirical relationships for ripple wavelength, height, and steepness, one for laboratory data and the other for field data. While these perform well within the range of conditions for which they were developed, neither adequately considers the full range of ripple response to wave conditions and they can yield values of ripple wavelength and height considerably in error when applied out of their range. The purpose of the work presented herein is to interpret laboratory and field measurements within a single framework and to construct a simple method for predicting ripple type, wavelength, and height applicable to both field and flume environments.

Observations of Wave-Generated Ripples

Beds of sand-sized sediment deform into ripples when subjected to oscillatory flows capable of initiating sediment motion. If the wavelength, L, of a surface gravity wave is less than about half the water depth, h, wave orbital motion will be present at the

Paper number 93JC02726.
0148-0227/94/93JC-02726$05.00

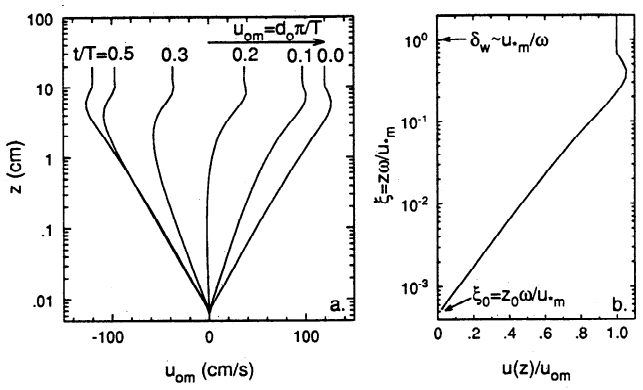

Fig. 1. (a) Example of velocity profiles in an oscillatory rough turbulent boundary layer over a half wave period. (b) Maximum velocity profile, normalized by maximum orbital velocity, u_{om}, as a function of nondimensional height above the bed, $\xi=z/\delta_w=z\omega/u_{*m}$. In this example, $u_{om}=120$ cm/s, $\omega=2\pi/T=0.524$ s^{-1}, $u_{*m}=7.8$ cm/s, and $z_0=0.007$ cm.

bed. For waves of small steepness, parameters such as wave orbital velocity and orbital diameter can be calculated using small-amplitude wave theory. In this case the diameter of the orbital motion just above the bed is given by $d_o = H/\sinh(kh)$, where H is wave height, h is water depth, and k is wave number, $2\pi/L$. The maximum near-bed wave orbital velocity associated with this orbital motion at the bed is $u_{om} = \pi d_o/T$, where T is wave period. Small-amplitude wave theory assumes that the bed is frictionless, but owing to the no-slip condition at the bed surface, a thin wave boundary layer exists in which the velocity increases from zero to the near-bed orbital velocity, u_o (Figure 1). As near-bed orbital velocity varies through a wave period, so does the velocity field in the wave boundary layer and the bottom shear stress (Figure 1).

The relationship between ripple spacing, λ, and orbital diameter, d_o, defined by field and laboratory measurements is shown in Figure 2a, in which both ripple spacing and orbital diameter have been nondimensionalized by mean diameter of the bed sediment; nondimensional ripple height, η/D, is shown for the same cases in Figure 2b. The data included in these figures are those for which both ripple wavelength and height were measured as a function of wave period, orbital diameter or orbital velocity, and grain size; we refer to these data as the primary data set. We also attempted to assure that the ripples were approximately in equilibrium with the flow by removing any cases in which the flow was significantly below threshold conditions for initiating sediment motion. If the estimated maximum shear velocity u_{*m} was less than $0.8u_{*cr}$, where u_{*cr} is the critical shear velocity for initial motion, the measurement was not included in the primary data set; the method used to determine u_{*m} is discussed later in the paper. Only data for quartz density beds have been used. The sources for the laboratory data are *Carstens et al.* [1969], *Mogridge and Kamphuis* [1972], *Dingler* [1974], and *Kennedy and Falcon* [1965]. Sources for field data are *Inman* [1957] and *Dingler* [1974]; significant wave height was used to determine d_o for field data. Data from oscillating bed experiments were not included (see discussions of *Miller and Komar* [1980a]; *Vongvisessomjai* [1984]).

The spacing of orbital ripples, which predominate at low values of d_o/D, is proportional to orbital diameter. *Miller and Komar* [1980a], using laboratory measurements of ripple wavelength for different sediment sizes and wave orbital diameters, proposed that for orbital ripples

$$\lambda_{orb} = 0.65 d_o \tag{1}$$

Anorbital ripples, which occur at relatively high values of d_o/D, have spacings that are essentially independent of d_o, but vary in roughly constant proportion to grain diameter [*Clifton and Dingler, 1984*]

$$\lambda_{ano} \simeq 400D - 600D \tag{2}$$

Ripples with spacings that fall between these limiting relationships are considered suborbital ripples. The relationships for the wavelength of orbital and anorbital ripples defined by (1) and (2) are indicated in Figure 2a.

Figure 3 shows our classification of these data as orbital, suborbital, or anorbital. The basis for our classification is described below. Comparison of Figures 2a and 3a reveals that most of the orbital ripples were observed in flumes, whereas most of the anorbital ripples were observed in the field. Suborbital ripples comprise both flume and field data. There are also differences in ripple height or steepness associated with the distinction between orbital and anorbital ripples; ripple steepness is shown in Figure 3b. Orbital ripples are characterized by a constant steepness of roughly 0.17. Anorbital ripples have maximum steepnesses smaller than this, closer to 0.12, and steepness decreases with increasing orbital diameter, until sheetflow conditions are reached (Figure 3b).

One of the questions that motivated this study is whether the differences between the characteristics of ripples measured in the laboratory and field are primarily a result of nonoverlapping wave conditions or fundamental differences in the dynamics of the two

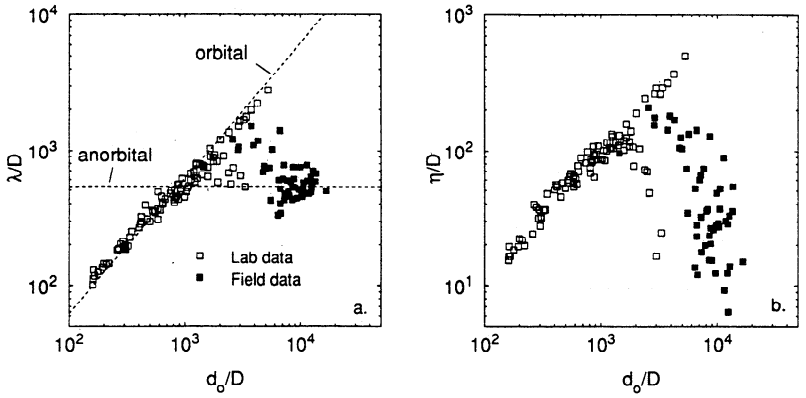

Fig. 2. Measured (a) ripple wavelength λ and (b) ripple height η, normalized by grain diameter D, as a function of normalized wave orbital diameter d_o/D from the laboratory studies of *Carstens et al.* [1969], *Kennedy and Falcon* [1965], *Mogridge and Kamphuis* [1972], and *Dingler* [1974] and the field studies of *Inman* [1957] and *Dingler* [1974]. The dashed lines in Figure 2a follow the observed trends for wavelength of orbital and anorbital ripples.

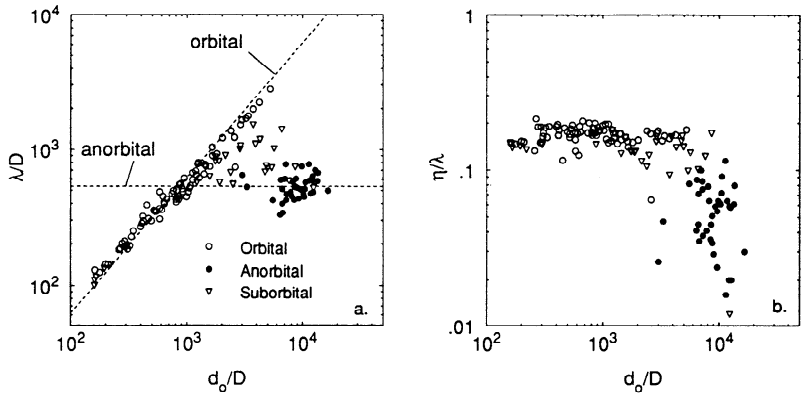

Fig. 3. Measured (a) ripple wavelength λ and (b) ripple steepness η/λ for the same cases shown in Figure 2, but with our classification of the ripples indicated by symbol type (see legend). The classification is based on equations (10a)-(10c).

environments. This question might be somewhat academic if we were certain that the combinations of wave parameters and sediment sizes that occur naturally on the continental shelf always yielded anorbital ripples. However, while anorbital ripples are most common on the shelf, a number of the field cases included in the primary data set appear to be suborbital, and there are even a few orbital ripples among the field data.

The likelihood of orbital and suborbital ripples forming on the continental shelf can be further investigated by determining combinations of water depth and wave height in which each type of ripple would be expected. To do this, we adopted the approximate criteria proposed by *Clifton and Dingler* [1984] that orbital ripples occur when $d_o/D < 2000$ and anorbital ripples are found when $d_o/D \approx 5000$ or larger. The ratio d_o/D is not a perfect discriminator, but it will suffice for showing the general distribution of ripple types. Given a grain size, D, values of d_o corresponding to $d_o/D = 2000$ and $d_o/D = 5000$ can be computed. For any value of wave height, H, the ratio H/d_o is related to water depth, h, through the relationship

$$kh = \ln\left[\frac{H}{d_o} + \left(\frac{H^2}{d_o^2} + 1\right)\right] \tag{3}$$

where k is wave number, $2\pi/L$, and L is the wavelength of a surface gravity wave. Water depth is then calculated from

$$h = \frac{gT^2}{4\pi^2} kh \tanh(kh) \tag{4}$$

for a given wave period. Any pair of h, H, and T can be related given the third parameter and d_o. Because wave period generally varies over a smaller range of values than does wave height and water depth on a given continental shelf, we specify period and relate h to H.

Curves delineating the combinations of water depth and wave height in which one would expect to find orbital, suborbital, and anorbital ripples are plotted in Figure 4 for three grain sizes spanning the fine to medium sand range: $D = 0.13$ mm, $D = 0.25$ mm, and $D = 0.5$ mm. For each grain size, periods of 8 s and 12 s were selected, representing characteristic wave periods for lower and higher energy shelves. In each case we assumed that water temperature is 10°C, sediment density is 2.65 g/cm^3, and fluid density is 1.0 g/cm^3. Four curves are shown for each grain size and period. The solid curves, labeled A, represent the suborbital/anorbital transition ($d_o/D = 5000$); anorbital ripples are found at combinations of h and H below and to the right of this curve, i.e., smaller water depths and larger wave heights. The dashed curves, labeled O, represent the orbital/suborbital transition ($d_o/D = 2000$); orbital ripples occur at combinations of h and H above and to the left of this curve, i.e., deeper water and smaller wave heights.

The dotted curves labeled C show the maximum water depths and minimum wave heights necessary to initiate sediment motion, based on values of critical orbital velocity, $(u_{om})_{crit}$, computed from critical shear stress for each sediment size (P.L. Wiberg, A theoretical investigation of boundary layer flow and bottom shear stress for smooth, transitional, and rough flow under waves, submitted to *Journal of Geophysical Research*, 1993) (hereinafter referred to as Wiberg (submitted manuscript)). The critical shear

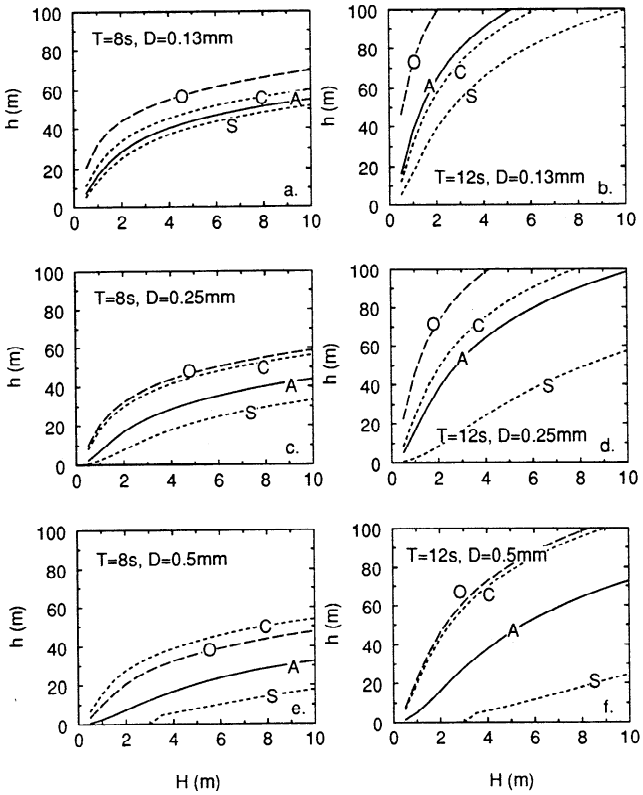

Fig. 4. Combinations of wave height H and water depth h in which orbital, suborbital, and anorbital ripples would be expected based on the criteria proposed by *Clifton and Dingler* [1984]: $d_o/D < 2000$ for orbital ripples; $d_o/D > 5000$ for anorbital ripples. (a) $D = 0.13$ mm, $T = 8$ s; (b) $D = 0.13$ mm, $T = 12$ s; (c) $D = 0.25$ mm, $T = 8$ s; (d) $D = 0.25$ mm, $T = 12$ s; (e) $D = 0.5$ mm, $T = 8$ s; (f) $D = 0.5$ mm, $T = 12$ s. The letter O indicates the limit for orbital ripples, A indicates the limit for anorbital ripples, C is the plane-bed initial motion limit, and S is the limit for full suspension.

stresses used as the basis for this calculation are plane-bed values and can only be considered approximate for a rippled bed, which would be expected to require higher values of u_{om} to produce threshold conditions at the bed surface owing to form drag. If the initial motion curve (C) lies within the anorbital ripple domain, e.g., Figure 4b, then no orbital or suborbital ripples should form in sediment of that size under waves of the specified period. The dotted curves labeled S indicate the combinations of water depth and wave height at which sediment of the given size would be expected to be in full suspension, in which case any small-scale ripples present on the bed would be expected to wash out; the condition used for full suspension is $w_s/(ku_{*m}) \approx 1.0$, where w_s is settling velocity and $k = 0.41$ is von Karman's constant.

As an example, we consider the $D = 0.13$ mm case at $h = 60$ m (Figures 4a and 4b). For the longer period, 12-s waves (Figure 4b), these calculations indicate that 2-m-high waves are required to initiate motion at this water depth, and that the ripples will always be anorbital. A wave height of 4 m appears to be sufficient to wash out the ripples, which would reform as anorbital ripples as wave height decreased. In contrast, waves with 8-s periods (Figure 4a) must be 10 m high just to initiate motion at this depth, implying that transport of 0.13-mm sediment occurs rarely, if ever, at these depths and wave periods. For a coarser bed with $D = 0.25$ mm and $T = 12$ s (Figure 4d), waves with heights of nearly 3 m are necessary to initiate transport, under which conditions the ripples would be expected to be suborbital. Waves over 4 m high would form anorbital ripples, and waves in excess of 10 m are necessary to fully suspend the bed material. The coarsest bed considered here (Figures 4e and 4f) is interesting because critical conditions occur at approximately the orbital/suborbital transition. Thus ripples forming at near critical conditions would have heights and spacings close to those expected for orbital ripples. Wave heights in excess of 6 m would be necessary for anorbital ripples to form in this case.

These results suggest that while anorbital ripples are the dominant ripple type on the continental shelf, suborbital ripples should also be present, particularly on medium sand and coarser beds, and that orbital ripples may be present on coarse sand beds.

Sediment Transport Conditions Under Waves

General Concepts

Ripple geometry depends significantly on the prevailing sediment transport conditions. Ripples develop during times when bed material is primarily moving as bed load. This precludes the occurrence of ripples on beds comprised entirely of sediment too fine to move as bed load (silts and finer). On sandy beds, ripples may wash out during high flow conditions when most of the moving bed material is carried in suspension but will reform as flow intensity wanes. Ripples formed during episodes of bed load transport persist during subcritical flows. On the continental shelf these tend to be slowly degraded by benthic organisms and occasional flows only large enough to move material at the ripple crests. The presence of these "relict" forms at subthreshold conditions complicates interpretation of field measurements of ripple geometry and must be considered in boundary layer calculations for the continental shelf [e.g., *Drake et al.*, 1992].

For sediment of a given size and density, wave conditions producing bed load, suspended load, or no sediment transport are a function of the boundary shear stress, τ_0, or shear velocity, $u_* = (\tau_0/\rho)^{1/2}$, exerted by the flow at the bed surface. In high-frequency oscillatory flows, such as those produced by surface gravity waves, the magnitude of the boundary shear stress depends on the near-bed wave orbital velocity, u_o, the height of the wave boundary layer, δ_w, and the bed roughness parameter, z_0, which is a function of k_s, the physical roughness scale of the bed. These parameters are illustrated in Figure 1b for the time of maximum near-bed wave orbital velocity, $u_o = u_{om}$. Wave boundary layer height is proportional to the ratio of maximum shear velocity, u_{*m}, over a wave cycle to wave frequency, $\omega = 2\pi/T$, i.e., $\delta_w \sim u_{*m}/\omega$; the constant of proportionality is of order 1. Shear velocity is related to the vertical gradient of velocity at the bed. As suggested in Figure 1b, the near-bed velocity gradient, and therefore shear velocity, increases as the difference in values between z_0 and δ_w decreases for a given u_{om}. Thus we could expect $u_{*m}/u_{om} = f(z_0/\delta_w)$. Here we adopt the notation $\xi_0 = z_0\omega/u_{*m}$. Velocity and shear stress vary through a wave period, but it is common to parameterize initial motion and suspension conditions under waves in terms of maximum boundary shear stress, τ_{0m}, or maximum shear velocity, u_{*m}.

Both experimental [e.g., *Jonsson*, 1963; *Jensen et al.*, 1989] and theoretical [e.g., *Kajiura*, 1968; *Smith*, 1977; *Grant and Madsen*, 1979; *Long*, 1981; *Trowbridge and Madsen*, 1984; Wiberg, submitted manuscript] approaches have been taken to the problem of relating near-bed orbital velocity to boundary shear stress or shear velocity. These studies have mostly concentrated on hydraulically rough flow ($R_* = u_* k_s/\nu > 70$–100) because of their prevalence in natural environments and the fact that the ratio u_{*m}/u_{om} or wave friction factor $f_w = 2(u_{*m}/u_{om})^2$ depends on just one independent variable under these conditions. Some of the data and relationships developed for the wave friction factor under rough oscillatory flow conditions are shown in Figure 5, including the *Jonsson* [1963] and *Jensen* [1989] wave tunnel data, the widely used semiempirical friction factor curve for rough flow of *Jonsson* [1963, 1966], the *Grant and Madsen* [1982] theoretical relationship for pure waves, and the Wiberg (submitted manuscript) theoretical curve. These curves can be used to estimate wave-generated boundary shear stress for rough turbulent flow given a_o/k_s, where the orbital amplitude $a_o = d_o/2$ and k_s is the physical roughness length of the bed; for a well-sorted planar bed, $k_s \approx D$, while for a rippled bed $k_s \approx 30\eta^2/\lambda$ [*Grant and Madsen*, 1982].

The relationship between shear velocity and orbital velocity is more complicated for hydraulically smooth ($R_* < 3$–5) and transi-

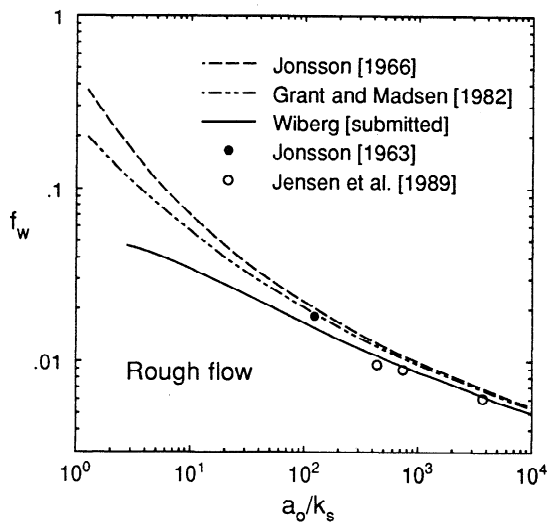

Fig. 5. Wave friction factor, f_w, as a function of a_o/k_s for rough turbulent flow. The symbols indicate measured values of f_w from *Jonsson* [1963] and *Jensen et al.* [1989]. The friction factor curves are from *Jonsson* [1966], *Grant and Madsen* [1982] and Wiberg (submitted manuscript).

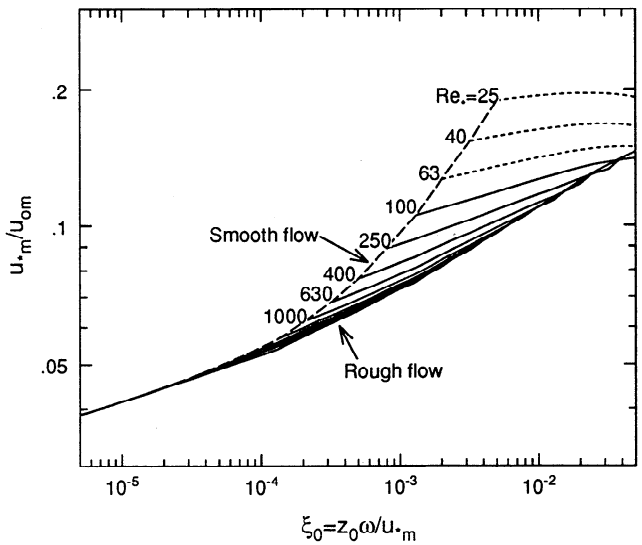

Fig. 6. Computed values of u_{*m}/u_{om} as a function of $\xi_0=z_o\omega/u_{*m}$ (Wiberg, submitted manuscript) for smooth, transitional, and rough turbulent oscillatory boundary layers. The curves correspond to a range of values of $Re_*=u_*^2/(\omega\nu)$. Rough flow and smooth flow limits are indicated. The boundary layer is laminar for Re_* less than roughly 100. These curves can be used to compute u_{om} given u_{*m}, ω, and z_0.

tional (intermediate values of R_*) flows because of the additional dependence of u_{*m}/u_{om} on a wave Reynolds number, which introduces effects of fluid viscosity into the problem. For these flows, $u_{*m}/u_{om} = f\,[\xi_0 = z_0\omega/u_{*m}$, $Re_* = u_{*m}^2/(\omega\nu)]$ or $u_{*m}/u_{om} = f\,[a_o/k_s$, $u_{om}^2/(\omega\nu)]$, depending on whether the known variable is u_{*m} or u_{om}. The theoretical relationship between u_{*m}/u_{om}, ξ_0, and Re_* for smooth, transitional, and rough turbulent flow computed by Wiberg (submitted manuscript) is shown in Figure 6. For a given shear velocity, bed roughness parameter z_0, and wave frequency ω, Figure 6 can be used to determine u_{om}. This is convenient, for example, for transforming a curve of critical shear stress to curves of critical orbital velocity (Wiberg, submitted manuscript). It is not as convenient for computing shear velocity or shear stress given orbital velocity, although this can be done iteratively. For rough flow, the relationship is a function of ξ_0 only, as noted above, which can be transformed to a_o/k_s assuming $k_s = 30z_0$ for rough flow. This is how the Wiberg curve in Figure 5 was obtained.

For given bed and wave conditions, computed values of wave-generated shear stress can be assessed for their transport potential. If the bed is rippled, however, some additional factors must be considered, and the problem is generally more difficult than for a planar bed of the same sediment type. Ripples increase the hydrodynamic roughness of a bed relative to grain roughness, and values of z_0 or k_s for ripples are not well established, although it appears that a reasonable estimate of the ripple-generated roughness parameter for symmetric ripples is given by the product of ripple height times ripple steepness, i.e., $z_{0r} = \eta^2/\lambda$ [see *Grant and Madsen*, 1982; *Wiberg and Nelson*, 1992]. The large values of bottom roughness associated with ripples can pose a problem for boundary shear stress calculations under waves because solutions to the unsteady boundary layer equations used to compute u_{*m}/u_{om} break down when the bed roughness parameter and boundary layer height are too close in value, i.e., $\xi_0 > 0.03$ (Wiberg, submitted manuscript). This is equivalent to $a_o/k_s \approx 8$, close to the limit of $a_o/k_s = 10$ suggested by *Jonsson* [1963], below which the assumptions for his friction factor formulation are violated.

Application to wave-formed ripple measurements

To examine the transport conditions corresponding to the data shown in Figures 2 and 3, u_{*m} was calculated for each case based on the formulation of Wiberg (submitted manuscript) used to construct Figure 6. The roughness parameter z_0 is initially set equal to the ripple roughness $z_{0r} = \eta^2/\lambda$. For most of the field cases, the value of $\xi_0 = z_{0r}\omega/u_{*m}$ was well below the upper limit of 0.03 noted above, and the calculation of u_{*m} was straightforward. However, the values of ξ_0 computed for most of the laboratory cases was significantly above this limit, and u_{*m} could not be reliably computed. This could have been anticipated if we had estimated values of a_o/k_s, the independent variable in the wave friction factor relationship (Figure 5), for the orbital ripple data. The steepness η/λ of orbital ripples is approximately 0.17, $\lambda_{orb} \approx 0.65d_o$, and $\eta_{orb} \approx 0.17\lambda_{orb}$. Combining these, we get $\eta_{orb} \approx 0.11d_o$, or $d_o/\eta_{orb} \approx 9$ for orbital ripples. Furthermore, $k_s \approx 30\eta^2/\lambda = 30(0.17\eta_{orb})$, so that $\eta_{orb} \approx 0.2k_s$. From this, we find that $5d_o/k_s \approx d_o/\eta_{orb} \approx 9$, or $a_o/k_s \approx 1$. This is well below the limiting value of 10 for reliable use of Jonsson's friction factor.

The physical significance of these results may be better understood if we relate $d_o = 2u_{om}/\omega$ to $\delta_w \approx u_{*m}/\omega$. The ratio $\delta_w/d_o = 0.5u_{*m}/u_{om}$. Because u_{*m}/u_{om} varies over a relatively small range of values for turbulent oscillatory flow ($Re_* > 100$ in Figure 6), d_o is roughly proportional to δ_w. Taking a representative value of u_{*m}/u_{om} equal to 0.08 (Figure 6), $d_o \approx 25\,\delta_w$. This

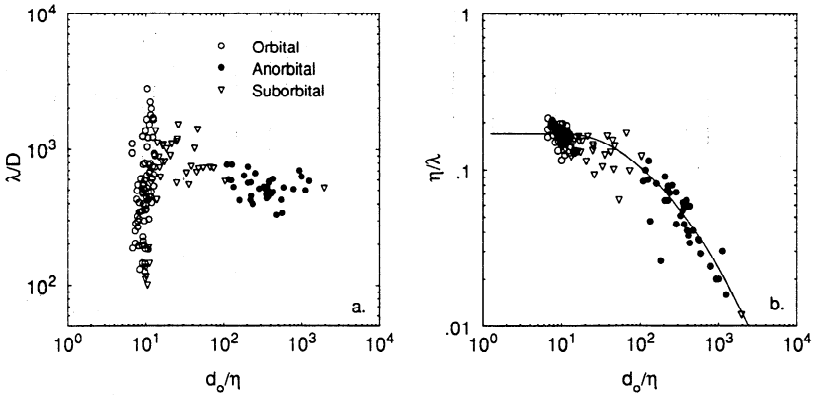

Fig. 7. Measured (a) ripple wavelength λ, normalized by grain diameter D and (b) ripple steepness η/λ as a function of the ratio of near-bed wave orbital diameter to ripple height, d_o/η, for the same cases shown in Figure 2. The curve in Figure 7b is a second-order polynomial fit to the steepness data and used to estimate steepness for anorbital and suborbital ripples in our calculations (equation (9)).

implies that for $d_o/\eta = 9$, the ratio δ_w/η is less than 1, that is bed form height exceeds the thickness of the wave boundary layer for orbital ripples. Values of ripple wavelength λ and steepness η/λ from the primary data set are plotted against measured values of the parameter d_o/η in Figure 7. As expected, the orbital ripple data all fall near $d_o/\eta = 9$. The anorbital data all have values of $d_o/\eta \geq 100$. The much larger values of d_o/η for anorbital ripples indicate that these are always well submerged within the wave boundary layer.

Following the arguments outlined above, we have tentatively defined orbital ripples as those with ripple heights greater than twice the thickness of the oscillatory boundary layer, that is, $\delta_w/\eta < 0.5$ or roughly $d_o/\eta < 12$. Anorbital ripples are defined as those for which ripple height is less than one-quarter of the boundary layer height, i.e., $\delta_w/\eta > 4$ or roughly $d_o/\eta > 100$. Ripples with ratios of δ_w/η falling between these values are regarded as suborbital ripples. This is the scheme used to classify the cases in the primary data set, as indicated in Figure 3.

Ripple heights significantly greater than the height of the wave boundary layer suggest that the wave boundary layer over orbital ripples may be discontinuous and transient, with a form roughly paralleling the ripple surface. Conceptually, this would be analogous to the viscous sublayer wrapping around bed roughness elements in hydraulically rough flow, in which case $k_s > 6$–$8\,\delta_v$; $\delta_v \approx 11.6\nu/u_*$ is the thickness of the viscous sublayer. Some evidence supporting this hypothesis can be found in oscillatory boundary layer measurements made by *Ikeda et al.* [1991] over a fixed, symmetric ripple. In these measurements, ripple height was 5 cm, ripple wavelength was 30 cm, period ranged from 3 to 9 s, and d_o varied from 20 to 40 cm; $d_o/\eta = 4$ to 8. Profiles of velocity and Reynolds stress, measured over a wave cycle, suggest that the observed turbulence is primarily associated with wake and vortex formation on the lee side of the ripple and that the wave boundary layer, to the extent that it is present, is thin compared to the scale of the ripple. However, it is likely that there is no persistent wave boundary layer in this case. Instead, there may be a growing internal boundary layer in contact with the bed downstream of the region of flow separation that is limited in height by the period of the oscillation and is disrupted each half wave cycle as the flow reverses.

If this is the case, the shear velocity u_{*m} for orbital ripples would depend on the bed surface roughness, z_{0sf}, rather than ripple roughness, z_{0r}, as well as wave or internal boundary layer thickness and potential flow velocity at the top of the boundary layer. There would be no region of spatially uniform, turbulent flow or shear stress as we assume exists above ripples well submerged in the wave boundary layer. The measurements of *Ikeda et al.* [1991] indicate that near-bed potential flow velocity on the upstream side of a ripple close to the crest has a value similar to the spatially uniform potential flow velocity above the ripple; potential velocity is much lower in the trough. Thus as a first approximation, we assume the average potential flow velocity above the ripples, u_{om}, is representative of the potential flow at the top of the wave boundary layer near the crest, where transport is likely to begin first. Potential flow theory could be used to generate an estimate of the spatially varying potential velocity at the top of the wave boundary layer, but it is not clear that this added level of sophistication is warranted in this analysis.

In light of these considerations, the u_{*m} we compute herein for orbital ripples is an estimate of the maximum shear velocity acting on the bed surface at the ripple crest, i.e., $(\tau_{sf})_{crest} \approx \rho u_{*m}^2$. The bed surface roughness parameter z_{0sf} is assumed to be the grain roughness of the mean bed size for a stationary bed [see *Schlichting*, 1979]; for a mobile bed, the bed load roughness parameter is calculated following *Wiberg and Rubin* [1989]. We use this estimate of u_{*m} both to characterize wave boundary layer height (u_{*m}/ω) and the shear velocity at the bed for sediment transport calculations. In contrast, we use two different values of shear velocity to compute wave boundary layer height and sediment transport for anorbital ripples. Maximum shear velocity, u_{*m} computed using ripple roughness provides an estimate of the "outer," spatially uniform shear velocity characteristic of the wave boundary layer flow above the ripples, and is used to compute wave boundary layer height. To estimate the shear velocity or shear stress at the bed surface for sediment transport calculations on anorbital ripples, a correction must be made for bed form drag, using a method such as that of *Einstein* [1950] or *Smith and McLean* [1977]. We used a modified form of the *Smith and McLean* [1977] bed form drag correction [*Wiberg and Nelson*, 1992],

$$\frac{\tau_0}{\tau_{sf}} = 1 + \frac{1}{2} C_D \frac{1}{k^2} \left[\ln \frac{\eta}{z_{0sf}} - 1 \right]^2 \frac{\eta}{\lambda} \tag{5}$$

where k=0.41 is von Karman's constant and C_D is a bed form drag coefficient. *Wiberg and Nelson* [1992] found $C_D \approx 1.0$ for undirectional flow over relatively sharp-crested, fixed symmetric ripples with geometries similar to those of wave-formed ripples.

The average shear stress at the bed surface computed from (5), τ_{sf}, is smaller than τ_0, the shear stress above the ripples. In addition, the actual value of shear stress at the bed surface varies with position over a ripple, with lower values in the broad troughs and higher values near the ripple crests. Thus sediment transport, when it begins, tends be localized at ripple crests. Based on the shear stress distributions over symmetric ripples measured by *Wiberg and Nelson* [1992], we have approximated the bed shear stress near the ripple crest for anorbital ripples as $(\tau_{sf})_{crest} = (1+12\eta/\lambda)\tau_{sf}$; for $\eta/\lambda = 0.125$, $(\tau_{sf})_{crest} = 2.5\tau_{sf}$ while in the limit of a flat bed, $\eta/\lambda = 0$ and $(\tau_{sf})_{crest} = \tau_{sf} = \tau_0$. For suborbital ripples, we compute shear stress following the procedure for anorbital ripples if $\xi_0 < 0.03$ and using that for orbital ripples for larger values of ξ_0.

Predicting Ripple Wavelength and Height

Using the view of the problem developed above, we have attempted to construct a more general method for predicting ripple height and wavelength than those currently available. We begin by assuming that the known parameters are grain size D, wave period T, and either orbital diameter d_o or wave height H and water depth h, which are related by the relationship $d_o = H/\sinh(kh)$; kh can be computed iteratively using the relationship $k_D h = kh \tanh(kh)$, where $k_D = 4\pi^2/(gT^2)$. These would be the known parameters if, for example, one were modeling boundary layer flow and sediment transport under specified wave conditions. The sedimentological problem is somewhat different, and will be considered later. There are two steps involved in our approach to predicting bed form characteristics: determining ripple type (orbital, anorbital, suborbital), and computing ripple dimensions based on ripple type and flow characteristics.

In the previous discussion it was argued that the most important difference between orbital and anorbital ripples is the ratio of wave boundary-layer thickness to ripple height, which can be approximated by the ratio d_o/η. If this ratio is small, the ripples are of the orbital type, and if the ratio is large, the ripples are anorbital (Figure 7). However, ripple height must be known before this ratio can be computed. Guided by previous work on this

problem, we have used our primary data set (Figure 3) to develop expressions for ripple wavelength and steepness for orbital and anorbital ripples. Ripple heights computed from these values provide upper and lower limits on the range of possible ripple heights and provide a starting point for our determination of the correct ripple type.

A best fit line fit through the orbital ripple data in Figure 3a gives

$$\lambda_{orb} = 0.62 d_o \tag{6}$$

and the average value of ripple steepness for the orbital ripple points in Figure 3b is

$$(\eta/\lambda)_{orb} = 0.17 \tag{7}$$

where the subscript "orb" indicates that the relationships apply to orbital ripples. In this case η_{orb} is readily obtained from the product of length and steepness given near-bed orbital diameter d_o.

A line fit through the anorbital ripple data in Figure 3a gives

$$\lambda_{ano} = 535D \tag{8}$$

although there is fair amount of scatter around this value; the subscript "ano" denotes anorbital ripples. Unlike orbital ripples, anorbital ripple steepness decreases with flow intensity, complicating estimation of ripple height. In several previous studies [*Nielsen*, 1981; *Grant and Madsen*, 1982] anorbital ripple steepness was parameterized in terms of nondimensional bed shear stress (skin friction). One could also argue that steepness might depend on Rouse number, $p_{sf} = w_s/ku_{*sf}$, since bed form steepness tends to decrease as the proportion of sediment in suspension increases. Although there are good arguments for using a u_*-based parameterization of ripple steepness, we found that ripple steepness is as well defined in terms of d_o/η (Figure 7b), which has the advantage of eliminating the complications and uncertainties of computing τ_{sf}. It also has the disadvantage that η appears on both axes so it must be solved for iteratively. The resulting relationship used to estimate the steepness of anorbital ripples is

$$\frac{\eta}{\lambda} = \exp[-0.095(\ln\frac{d_o}{\eta})^2 + 0.442\ln\frac{d_o}{\eta} - 2.28] \tag{9}$$

for $d_o/\eta > 10$; if $d_o/\eta \le 10$, $\eta/\lambda = 0.17$. The curve given by (9) is plotted with the data in Figure 7b.

To determine ripple type, orbital and anorbital ripple heights (η_{orb} and η_{ano}) are computed for each case from the above expressions. In the previous section the criteria $\eta/\delta_w > 2$ for orbital ripples and $\eta/\delta_w < 0.25$ for anorbital ripples were suggested, which are approximately equivalent to $d_o/\eta < 12$ and $d_o/\eta > 100$, respectively. The ratio of d_o to anorbital ripple height η_{ano} is used to establish ripple type, because the ratio d_o/η_{orb} given by (6) and (7) is constant for all wave and sediment conditions. The ability of these criteria to discriminate ripple type within the primary set of data is indicated in Figure 8 in which d_o/η_{ano} is plotted against the Rouse number, $p_{sf} = w_s/ku_{*sf}$, also computed assuming the ripples are anorbital. The anorbital limit, $d_o/\eta_{ano} > 100$ correctly classifies almost all of the anorbital points, as expected. The orbital limit of $d_o/\eta_{ano} < 12$ is less successful because the criterion was established based on orbital ripple height and this calculation uses anorbital ripple height. A criterion of $d_o/\eta_{ano} < 20$ correctly classifies more of the orbital ripples without misclassifying too many suborbital ripples, so we adopt this limit. Thus the criteria used in the calculations are

$$d_o/\eta_{ano} < 20 \qquad \textit{orbital ripples} \tag{10a}$$

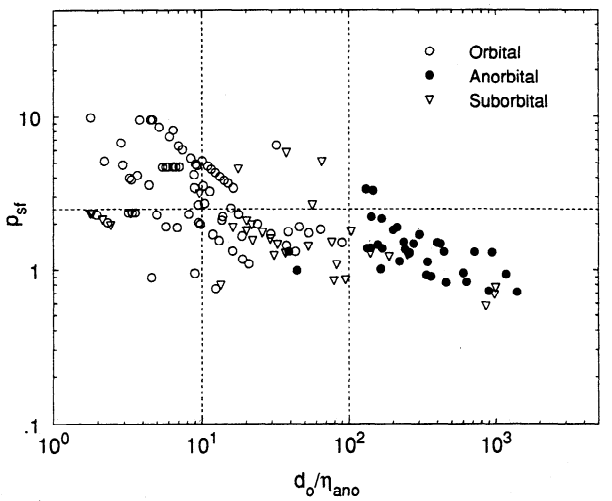

Fig. 8. Measured ripple data, classified according to type (see legend), plotted in terms of the ratio of near-bed orbital diameter to predicted anorbital ripple height, d_o/η_{ano} and Rouse number $p_{sf} = w_s/(ku_{*sf})$. The horizontal dotted line indicates $p_{sf} = 2.5$, the approximate criterion for incipient suspension of bed load sediment. The vertical lines indicate the criteria for orbital and anorbital ripples developed from the data.

$$d_o/\eta_{ano} > 100 \qquad \textit{anorbital ripples} \tag{10b}$$

$$20 < d_o/\eta_{ano} < 100 \qquad \textit{suborbital ripples} \tag{10c}$$

It is interesting to note in Figure 8 that the Rouse number, p_{sf}, is less than 2.5 for almost all anorbital ripples, indicating that some portion of the bed sediment is at least incipiently suspended in most of these cases.

Ripple spacing and steepness for ripples classified as orbital or anorbital are given by (6)-(9); ripple height is computed from the product of wavelength and steepness. Suborbital ripples have wavelengths that fall between the orbital and anorbital limits. To estimate wavelength for these ripples we took a weighted geometric average of the bounding values λ_{ano} and λ_{orb}, so that

$$\lambda_{sub} = \exp\left[\left[\frac{\ln(d_o/\eta_{ano}) - \ln 100}{\ln 20 - \ln 100}\right](\ln\lambda_{orb} - \ln\lambda_{ano}) + \ln\lambda_{ano}\right] \tag{11}$$

This gives $\lambda_{sub} = \lambda_{ano}$ when $d_o/\eta_{ano} = 100$; $\lambda_{sub} = \lambda_{orb}$ when $d_o/\eta_{ano} = 20$. Ripple steepness and height are estimated using (9) and (11). This simple scheme for estimating suborbital ripple properties appears to be adequate for relating ripple wavelength and height to general wave and sediment characteristics, but may not be ideal for estimating a time series of ripple properties owing to the sharp changes in the slope of the relationship for ripple wavelength at the orbital/suborbital and anorbital/suborbital transitions, i.e., $d_o/\eta_{ano} = 20$ and $d_o/\eta_{ano} = 100$. A smoother cubic function for λ_{sub} that is continuous with the relationships for orbital and anorbital wavelength might be more appropriate for time-dependent calculations.

Predicted ripple wavelengths and heights for our primary data set are compared with the measured values in Figure 9. This is not an independent test of our method since these data were used to construct equations (6) through (9), but it indicates the amount of the variation in the data we are able to account for with these simple relationships. The wavelength predictions (Figure 9a) are more accurate than the height predictions (Figure 9b). The scatter about the line of perfect agreement in Figure 9b is largely the result of scatter about the regression between steepness and d_o/η used for the anorbital calculations (Figure 7b). The scatter exhi-

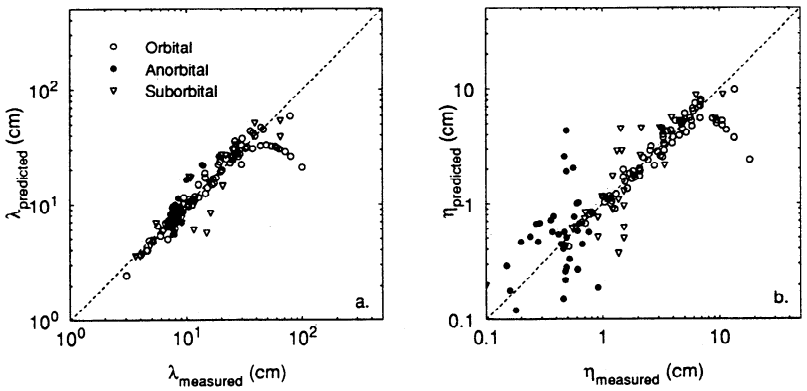

Fig. 9. Predicted versus measured ripple (a) wavelength and (b) height for the primary data set (data shown in Figure 2) using the method described herein (equations (6)-(11)). The dotted lines are the lines of perfect agreement.

bited by some suborbital points is the result of misclassification. For all points in the primary data set, 89% of the orbital ripples were correctly identified as orbital in the predictions; 82% of the anorbital ripples, and 48% of the suborbital ripples were correctly classified. Five cases included in the data set were designated by the investigator as upper plane bed, or sheetflow, cases. Of these, three were predicted to be upper plane bed, based on a criterion of computed steepness being less than 0.01.

Although all of the available ripple data that included measurements of ripple wavelength and height were used to construct our primary data set, we can use measurements lacking ripple height, which were left out of the primary data set, to compare predicted and measured ripple wavelength for flume and field cases. These data cannot be used to test the ripple classification scheme because classification of the observed ripples depends on measured ripple height. This second, independent set of ripple measurements includes the laboratory flume measurements of *Yalin and Russell* [1962] and *Miller and Komar* [1980a], as well as the field measurements of *Miller and Komar* [1980b] and the *Inman* [1957] data that lacked values for ripple height (the rest of the *Inman* [1957] data are in the primary data set). The *Miller and Komar* [1980b] data include measurements made under wave conditions in which a significant amount of wave energy was present at two, and in one case three, discrete frequencies, probably as a result of combined locally generated sea and remotely generated swell. Orbital diameters for the component wave frequencies are connected by lines in Figure 10; components with orbital velocities less than 80% of the estimated critical orbital velocity for initial motion were not included.

Nondimensional ripple wavelength λ/D is plotted against d_o/D in Figure 10a, with the lines for orbital and anorbital ripple wavelength given by (6) and (8). While these ripples could not be classified by type as noted above, their placement relative to the orbital and anorbital ripples line in Figure 10a is suggestive of ripple type. Measured and predicted wavelengths are compared in Figure 10b. The points at $\lambda_{predicted} = 8.8$ cm indicate the predicted anorbital ripple spacing for the *Miller and Komar* [1980b] field data. A number of corresponding measured ripple wavelengths fall close to this value, but some are significantly higher. For many of the multiple wave frequency cases in the *Miller and Komar* [1980b] data, the ripples were classified as anorbital for each component wave period, resulting in a single value for predicted spacing. In the other cases, the ripples corresponding to the lower values of orbital diameter were suborbital, while the higher orbital velocities indicated anorbital ripples. In all cases of multiple-peaked spectra, the frequency component with the largest orbital velocity was associated with the largest proportion of wave energy. As a result, one might expect that these components would control the ripple geometry. However, the agreement between measured and predicted ripple type was not improved if only these components of the *Miller and Komar* [1980b] field data set were compared.

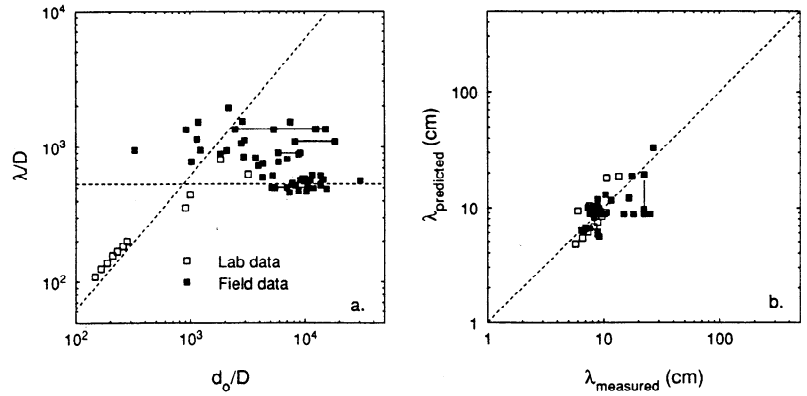

Fig. 10. (a) Measured ripple wavelength λ normalized by grain diameter D, as a function of normalized wave orbital diameter d_o/D from the laboratory studies of *Yalin and Russell* [1962] and *Miller and Komar* [1980a], the field studies of *Miller and Komar* [1980b], and the field measurements of *Inman* [1957] that lacked values for ripple height. The horizontal lines connect the values of d_o associated with peaks in multiple-peaked wave spectra measured in some cases by *Miller and Komar* [1980b]. (b) Predicted versus measured ripple wavelength for the data shown in Figure 10a. The dotted line is the line of perfect agreement. These data could not be classified because ripple height was not available in most cases.

Recently, a new series of measurements of ripples formed in oscillatory flow ducts was made by *Southard et al.* [1990]. These data are particularly interesting for the very long wavelength ripples that formed under high flows in fine-medium sand. The majority of measurements were made in a small duct (10 cm wide, 25 cm deep, and 6 m long) using water heated to 50°-70°C, which made it possible to generate oscillatory motions with 10°C-equivalent periods ranging from 3-20 s [*Southard et al.*, 1990]. A second set of measurements was made in a larger duct (40 cm wide, 26 cm deep, and 15 m long) to facilitate accurate measurements of larger bed forms. The observed bed forms had two- and three-dimensional crestline geometries and wavelengths that exceeded 1 m when orbital diameter was large, often with superimposed smaller ripples.

The *Southard et al.* [1990] measurements are somewhat difficult to interpret in the context of the present analysis. The largest bed forms in the small duct had wavelengths much longer than the flume width, creating the possibility that flume scales interfered with the ripple scales. The measurements in the wider flume were undertaken to avoid this problem [*Southard et al.*, 1990]; these measurements are summarized in Table 1. The wide-duct set of measurements began with flows having moderate orbital diameters. Both observed ripple wavelengths (~15 cm) and predicted values (~10 cm) under these conditions would be classified as suborbital (Runs 2-1 to 2-8, Table 1). As orbital diameter was increased, smaller ripples with spacings of 6-8 cm and heights of roughly 1.5 cm were observed superimposed on low relief, larger-scale forms with with spacings of the order of 1 m. The smaller ripples are consistent with anorbital ripple wavelengths and heights predicted for these wave conditions. The spacing of the larger forms is close to that expected for an orbital ripple in the given flow ($\lambda_{orb} \approx 1$ m for $d_o \approx 1.6$ m). Still higher values of d_o resulted in more pronounced large-scale ripples with spacings of the order of 1-2 m and heights of roughly 15 cm, with small superimposed ripples becoming limited to the troughs and on the flanks of the larger forms [*Southard et al.*, 1990]. Under these flow conditions, the calculations indicate upper plane bed or sheetflow conditions. The larger forms continue to have spacings generally consistent with orbital ripples.

One interpretation of these measurements is that orbital and anorbital ripples were both present during runs 2-10 to 2-15 (Table 1). The wavelength of the small-scale superimposed ripples apparently remained fairly constant, with $\lambda = 6$–8 cm. This spacing and the high flow conditions are consistent with these being anorbital ripples. The spacing of the larger forms is consistent with that expected for orbital ripples, but in this case, the flow conditions are not. Listed in Table 1 are estimated values of shear velocity u_{*sf}, computed as described above. While these can only be considered rough estimates, calculations of the ratio of estimated wave boundary layer height to measured ripple height, δ_w/η_{meas}, and Rouse number $p_{sf} = w_s/(ku_{*sf})$ reveal some interesting trends. Values of the Rouse number p indicate that a significant fraction of the bed material should be moving as suspended load, especially near the crests where the boundary shear stresses are highest. This is corroborated by the observations that the crests of the larger forms were rounded and that smaller-scale ripples were only found in the troughs and flanks [*Southard et al.*, 1990]. Furthermore, the ratio of wave boundary layer height to ripple height for the larger forms is significantly less than 1 in most cases and supports the interpretation that they are orbital bed forms. These seemingly inconsistent observations (orbital ripples forming under conditions of high sediment suspension and large orbital diameter) might be explained if the suspended material was largely confined to a relatively thin, high concentration layer near the bed, such that the mean travel distance of suspended particles is less than the orbital ripple wavelength and that small decreases in shear stress cause deposition. The relatively shallow, confined depths of the flume in the Southard et al. experiments may have contributed to the formation of the larger bed forms.

Comparison With Other Expressions for Ripple Scales

Grant and Madsen [1982] and *Nielsen* [1981] have proposed expressions for the wavelength, height, and steepness of ripples formed under oscillatory flows. *Nielsen* [1981] developed separate expressions for laboratory and field conditions based on measurements collected from a wide range of sources. He argued

TABLE 1. Measured and Computed Characteristics of Oscillatory Bed Forms Measured by *Southard et al.* [1990]

Run	D, mm	u_o*, cm/s	d_o, cm	T*, s	λ_{meas}†, cm	η_{meas}†, cm	$(u_*)_{calc}$, cm/s	δ_w/η_{meas}	p
2-1	0.11	26	50	6.0	15	2.6	1.7	0.6	1.2
2-2	0.11	20	38	6.0	13	2.0	1.4	0.7	1.4
2-4	0.11	22	60	8.5	20	2.5	1.4	0.8	1.4
2-5	0.11	17	46	8.5	16	1.2	1.2	1.4	1.6
2-6	0.11	18	49	8.5	15	1.2	1.3	1.4	1.5
2-7	0.11	34	92	8.5	7	1.0	2.0	2.7	1.0
2-8	0.11	25	68	8.5	14	2.2	1.6	1.0	1.2
2-9	0.11	42	114	8.5	7	1.0	2.3	3.1	0.9
2-10	0.11	51	138	8.5	7‡	1.0‡	5.0	6.8	0.4
2-10	0.11	51	138	8.5	100§	2.7§	2.6	0.7	0.7
2-11	0.11	57	154	8.5	120	20	2.9	0.2	0.7
2-12	0.11	60	162	8.5	120	20	3.1	0.2	0.6
2-13	0.11	74	200	8.5	150	12	3.6	0.4	0.5
2-14	0.11	83	225	8.5	200	12	4.0	0.5	0.5
2-15	0.11	88	238	8.5	200	10	4.2	0.6	0.5
2-16	0.11	100	271	8.5	220	3.0	7.9	3.6	0.3

* Values of u_o and T are adjusted to 10°C, as given in Table 2 of *Southard et al.* [1990]; d_o is computed from u_o and T.
† Average values of measured wavelength and height taken from Table 2 and the Appendix of *Southard et al.* [1990].
‡ Small-scale superimposed ripple wavelength and height for Run 2-10.
§ Large-scale ripple wavelength and height for Run 2-10.

that ripple steepness should be a function of nondimensional shear stress $\tau_* = \tau_0/[(\rho_s-\rho)gD]$ (Shields parameter) and parameterized ripple wavelength and height, both nondimensionalized by orbital amplitude a_o, in terms of what *Nielsen* [1981] called the mobility number, $\psi = \rho u_o^2/[(\rho_s-\rho)gD]$; ψ is different from τ_* by a factor of $(u_{*m}/u_{om})^2$. *Nielsen* [1981] computed the ratio u_{*m}/u_{om} using an expression for wave friction factor with a physical roughness length $k_s = 2.5D$, so that τ_* represents skin friction; *Nielsen's* [1981] friction factor curve is essentially the same as *Jonsson's* [1966], shown in Figure 5. Fitting curves to the data, Nielsen obtained

$$\eta/\lambda = 0.182-0.24\tau_*^{3/2} \quad (12a)$$

$$\lambda/a_o = 2.2-0.345\psi^{0.34} \quad (12b)$$

$$\eta/a_o = 0.275-0.022\psi^{1/2} \quad (12c)$$

for laboratory data; and

$$\eta/\lambda = 0.342-0.34\tau_*^{1/4} \quad (13a)$$

$$\lambda/a_o = \exp[(693-0.37\ln^8\psi)/(1000+0.75\ln^7\psi)] \quad (13b)$$

$$\eta/a_o = 21\psi^{-1.85} \quad (\psi>10) \quad (13c)$$

for field data; the expressions for ripple height are based on quartz density sediment only.

Grant and Madsen [1982] developed empirical relationships for ripple steepness and height (η/a_o) expressed as a function of transport stage, $\tau_{*sf}/(\tau_*)_{cr}$, that is, the ratio of nondimensional bed shear stress (skin friction) to the nondimensional critical shear stress for initiating sediment motion. Primarily using the *Carstens et al.* [1969] laboratory study of oscillatory ripples, *Grant and Madsen* [1982] suggested

$$\eta/\lambda = 0.16(\tau_{*sf}/(\tau_*)_{cr})^{-0.04} \quad (14a)$$

$$\eta/a_o = 0.22(\tau_{*sf}/(\tau_*)_{cr})^{-0.16} \quad (14b)$$

for values of transport stage less than what *Grant and Madsen* [1982] call the breakoff point, i.e., $\tau_{*sf}/(\tau_*)_{cr} < [\tau_{*sf}/(\tau_*)_{cr}]_B$; this was termed the equilibrium range and roughly corresponds to what we are calling orbital ripples. At higher transport stages, in the "breakoff range," *Grant and Madsen* [1982] found

$$\eta/\lambda = 0.28S_*^{0.6}(\tau_{*sf}/(\tau_*)_{cr})^{-1} \quad (15a)$$

$$\eta/a_o = 0.48S_*^{0.8}(\tau_{*sf}/(\tau_*)_{cr})^{-1.5} \quad (15b)$$

where $S_* = [(\rho_s/\rho)-1]gD^{3/2}/4\nu$ is a dimensionless grain parameter. The breakoff point is given by $[\tau_{*sf}/(\tau_*)_{cr}]_B = 1.8S_*^{0.6}$ [*Grant and Madsen*, 1982]. Wave orbital amplitude and skin friction are related via the Grant and Madsen friction factor relationship shown in Figure 5.

The Nielsen and Grant and Madsen relationships for ripples utilize both the wave orbital amplitude, a_o, and skin friction, τ_{sf}, which are related through a wave friction factor. Thus for both methods, ripple height, wavelength, and steepness are completely specified given a_o, wave period, T, mean grain size, D, sediment and fluid density, and fluid temperature. This set of parameters also provides the information necessary to compute ripple properties using our method, suggesting that an appropriate basis for intercomparison of these relationships would be orbital amplitude or orbital diameter. The three relationships for ripple wavelength and steepness as a function of orbital diameter are compared in

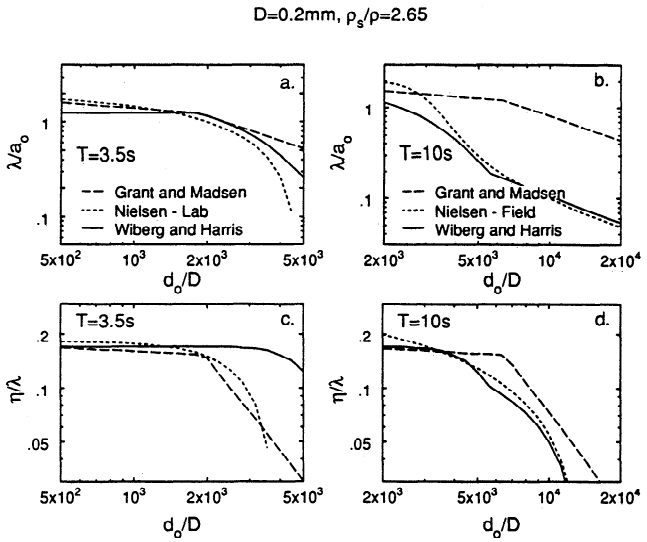

Fig. 11. Comparison of the predicted relationships for (a, b) ripple wavelength, normalized by orbital amplitude $a_o=d_o/2$, and (c, d) ripple steepness as a function of d_o/D computed using the methods of *Nielsen* [1981], *Grant and Madsen* [1982], and the method described in this paper. The calculations were made for quartz-density, 0.2 mm diameter sand; a water density of 1.0 g/cm^3 and a water temperature of 10°C were assumed. Results are shown for wave periods of 3.5 s (Figures 11a and 11c) and 10 s (Figures 11b and 11d), representative of laboratory and field waves.

Figure 11 for 0.2 mm, fine quartz sand; when computing these curves, we assume fluid density is 1.02 g/cm^3 and water temperature is 10°C. Comparisons are shown for wave periods of T=3.5 s and T=10 s, representative of laboratory and field conditions; Nielsen's laboratory expressions (12) were used when T=3.5 s and his field relationships (13) were used when T=10 s. Based on estimates of critical shear stress for initial motion and for full suspension of 0.2-mm quartz sand, the range of values of d_o/D for bed load transport is roughly 900-3000 when T=3.5 s; if T=10 s, the range of d_o/D is roughly 3000-10,000. These ranges define the conditions under which ripples would be active and indicate that the T=3.5 s ripples are orbital and suborbital, whereas the T=10 s ripples are suborbital and anorbital.

At lower wave periods (T=3.5 s), the three methods give similar relationships for ripple length over the range of d_o/D in which ripples are active. This agreement could be expected inasmuch as the orbital ripples observed and predicted to dominate at these low periods are the best defined observationally. The Nielsen and Grant and Madsen curves for ripple steepness for T=3.5 s also give similar relationships for the decrease in ripple steepness at higher values of d_o/D. Our method appears to overpredict the steepness of suborbital ripples at these low wave periods which are representative of laboratory conditions. At higher wave periods (T=10 s), when the ripples are suborbital to anorbital, Nielsen's relationship and ours for ripple wavelength are very close; the Grant and Madsen relationship yields much longer wavelengths. All three relationships for steepness when T=10 s are similar, although the Grant and Madsen relationship yields somewhat higher values of steepness than the other two methods.

Figure 12 shows the results of applying the predictions of the *Nielsen* [1981] and the *Grant and Madsen* [1982] expressions to our primary data set, and, with Figure 9, provide some sense of the strengths and weaknesses of the various methods. The *Grant and Madsen* [1982] expressions closely predict orbital and many suborbital ripple spacings and heights but significantly overpredict spacings and heights for anorbital ripples. Nielsen's method

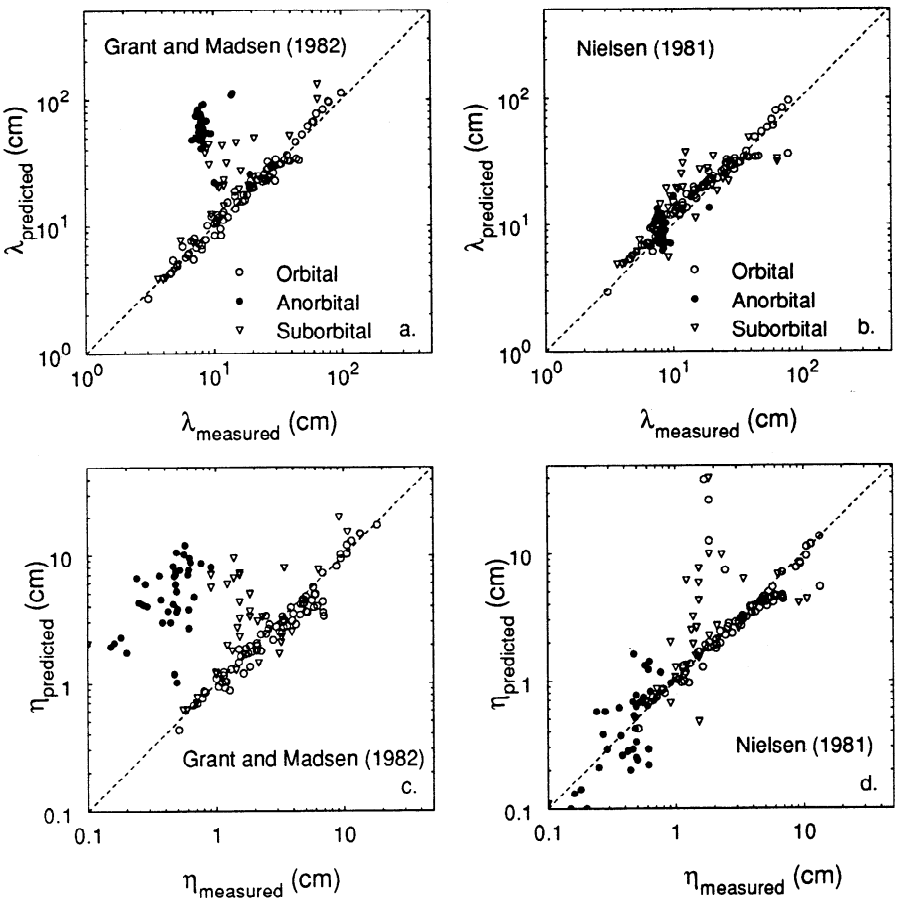

Fig. 12. Measured ripple wavelength λ and ripple height η versus predicted values computed for the primary data set (see Figure 3) using the expressions of (a, c) *Grant and Madsen* [1982] and (b, d) *Nielsen* [1981]. The dotted line is the line of perfect agreement.

yields wavelengths in close agreement with the data and values comparable to our predicted wavelengths, with the exception of a series of flume measurements of relatively long wavelength orbital ripples from *Mogridge and Kamphuis* [1972]. Our method indicates that these ripples should be suborbital (open circles falling below the line of perfect agreement in Figure 9), whereas the measurements show that they continue to have spacings and height consistent with orbital ripples. Nielsen's expressions for laboratory conditions provide a better estimate of λ and η for these ripples. Comparison of measured ripple heights to predicted values computed using our method and Nielsen's equations indicate roughly comparable performance. Nielsen's method significantly overpredicts ripple height for some orbital and suborbital cases, whereas our method results in a larger scatter of values for anorbital ripple height. Part of the error in our method is attributable to improperly classifying ripple type. Some of the error in Nielsen's method may result from the classification of ripples by environment rather than by ripple type.

Field Example

An interesting test of these methods for predicting ripple scales is provided by some recent bottom boundary layer measurements made on the northern California inner continental shelf just north of the Russian River as part of STRESS, a continental shelf sediment transport study. Bottom characteristics of the inner shelf study area vary considerably over relatively short distances [*Cacchione et al.*, 1984, 1987]. In regions where rocky promontories are present at the shoreline, the bottom exhibits large, low-relief crescentic dunes of fine sand underlain by coarse sand and shell fragments. In some areas large-scale ripples (spacings > 50 cm) are present in the coarser sediment. Between the rocky promontories and on the dunes, the bed is characterized by fine sand molded into small-scale symmetric ripples (spacings of roughly 10-15 cm). The wide variation in bottom ripple scales under essentially identical wave conditions provides a good test of the methods available for predicting ripple type. Wave orbital velocities determined from significant wave height measured during these deployments by the Geoprobe bottom tripod [*Cacchione and Drake*, 1979] ranged from 10 to 55 cm/s with periods of 12-16 s. The highest wave conditions could suspend the fine sand, while moderately high wave conditions are necessary to initiate motion of the coarse sand.

Selecting representative wave conditions from the time series that were sufficient to mobilize the bed material but not so high as to suspend sediment of the mean size, we computed predicted wavelengths for these ripples using the three methods discussed above. The input wave conditions and results are listed in Table 2. The observed ripple spacing on the fine-medium sand bed (D = 0.25 mm) is the expected spacing for anorbital ripples. Our method and *Nielsen's* [1981] predict ripple wavelengths of the correct order, although ripples as large as the Nielsen value of 20 cm were rare in bottom photographs. The *Grant and Madsen* [1982] method results in considerable overestimation of ripple wavelength. Close estimation of the actual wavelength for the coarse sand bed was difficult to make because in many cases there was only one crest in the camera's field of view; in some cases,

TABLE 2. Measured and Predicted Ripple Wavelengths at the STRESS Inner Shelf Site, Northern California

h, m	D, mm	τ_{cr}, dyn/cm^2	u_o, cm/s	T, s	$\lambda_{observed}$, cm	λ_{WH},* cm	λ_{GM},† cm	λ_N,‡ cm
54	0.25	2.2	40	14	12-15	13	107	20
54	0.65	3.3	50	15	>50	63	140	48

* Ripple wavelength computed using the Wiberg and Harris method described in this paper.
† Ripple wavelength computed using the *Grant and Madsen* [1982] method.
‡ Ripple wavelength computed using the *Nielsen* [1981] method for field conditions.

however, two crests were visible (D.A. Cacchione, personal communication, 1992). The field of view is roughly 80 cm, so we can conclude that the features are >50 cm in wavelength, and at least some of the ripples are <100 cm, but the average spacing is unknown. In this case our method predicts suborbital ripples with spacings of roughly 60 cm, which may be on the low side. Nielsen's method for field conditions yields still smaller wavelengths. The Grant and Madsen method predicts spacings that are much higher, close to orbital ripple spacings for these waves. These values are probably high.

Application to Hydrodynamic Interpretation of Shallow Marine Deposits

One of the motivations for studying the relationship between wave parameters and the characteristics of ripples on the underlying beds is the possibility of reversing the logic to infer wave parameters from bed form characteristics preserved in shallow marine deposits. Most wave-formed ripples on the continental shelf fall in the anorbital and suborbital classes (Figure 4), thus it is generally not possible to directly relate ripple wavelength to orbital diameter as one could for orbital ripples. When reconstructing the hydrodynamic environment associated with anorbital or suborbital ripples, critical shear stress is the strongest piece of evidence available. Another important sediment transport threshold is the transition from a rippled bed to upper plane bed conditions. As discussed earlier, shear velocity can be related to orbital velocity, and orbital velocity can be related to combinations of water depth and wave height for a given wave period and bed sediment size (Figure 4). As illustrated in Figure 4, the initial motion and suspension curves define a range of water depth and wave height over which active ripples will exist on the bed. Likely ranges of wave periods can then be used to narrow the range of possible depths.

As an example, we consider a section from the Elkton siltstone of southwestern Oregon. This Eocene-age unit has been interpreted by *Dott and Bird* [1979] as a shelf or slope sequence, deposited in front of the advancing Coaledo delta. Figure 13 is a line drawing (J. Bourgeois, personal communication, 1986) of one section of this deposit. It includes wave ripple structures showing distinct internal lamination above what appears to be an erosional contact and which change about halfway up the section into vertically climbing ripples that suggest draping by sediment settling out of suspension. The ripples are about 10 cm long and 1-1.5 cm high, with an average grain size of roughly 0.2 mm (J. Bourgeois, personal communication, 1986). The bottom half of the section clearly indicates active bed load transport, with a likely drop to subcritical shear stresses higher in the section where the ripples climb vertically and the laminae become nearly parallel. There is a suggestion of near-parallel bedding above the erosional base that may indicate transport conditions approaching upper plane bed at the bottom of the section. Generally the sequence is consistent with a waning-flow storm deposit.

Curves showing the combinations of water depth and wave height necessary to produce orbital velocities sufficient to initiate sediment motion (planar bed values) and fully suspend the bed material are shown in Figure 14, assuming a wave period of 12 s, typical of moderate swell on the Oregon continental shelf. As indicated by the horizontal lines, the depth of water necessary for initial motion under a 3-m-high wave (3m-IM) and full suspen-

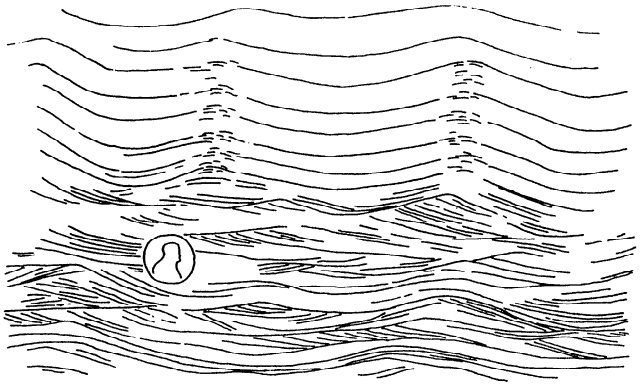

Fig. 13. Line drawing of a section from the Elkton siltstone, an Eocene-aged deposit from southwest Oregon. The drawing was made by Joanne Bourgeois from a photograph of the section. The mean sediment size for the section is approximately 0.2 mm. The ripple spacing is roughly 10 cm and ripple heights average 1.0-1.5 cm. The scale is a penny.

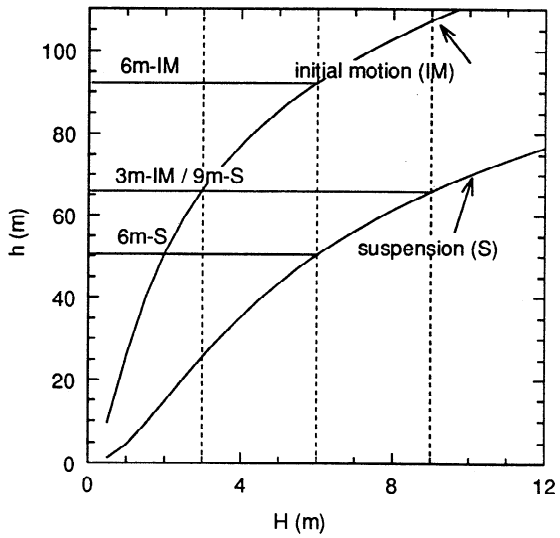

Fig. 14. Constraints on the depth of the Elkton deposit (Figure 13) at the time of formation based on combinations of wave height H and water depth h necessary to initiate sediment motion and to fully suspend sediment of the average bed size.

sion under a 9-m (9m-S) wave is about 65 m. Initial motion for 6-m-high waves occurs at roughly 92 m and suspension at about 50 m. A 3-m-high wave on today's Oregon coast would be considered a typical storm wave, a 6-m-high wave would be a large storm wave, and a 9-m wave would be an extreme wave. Because there is little evidence of parallel bedding in this section, or elsewhere in the upper Elkton (J. Bourgeois, personal communication, 1986), it is likely that the depth at which the deposit was formed was greater than the depth corresponding to full suspension for the larger waves, so that $h > 50$–60 m. This suggests there was little or no transport occurring on the bed during nonstorm conditions because the water depth is approaching the value at which even normal storm waves could not generate stresses large enough to initiate sediment motion. This is also consistent with the apparent lack of bed load transport during deposition in the upper part of the section in Figure 13. On the other hand, bed load transport clearly was occurring in the lower part of the section, so the depth must be shallower than the maximum depth for initial motion of the bed material under large 6-m storm waves, that is, $h < 92$ m. If the sequence of bedding is considered, the deposit must have formed at a depth at which the large storms waves were capable of transport approaching upper plane bed conditions, moderate waves could transport sediment as bed load, and the waves that followed the storm could not move the bed material. Shelf depths of the order of 65 m ±10 m or so are most consistent with these constraints for the Elkton deposit based on these calculations.

DISCUSSION

The results of our analysis suggest that the ripples observed in laboratory flumes and in the field can be interpreted within a common framework. This framework provides a method for classifying ripples as orbital, anorbital, or suborbital, based on ripple height and near-bottom wave orbital diameter, and for predicting ripple wavelength and height based on the grain size of the bed sediment and wave orbital diameter. As others have noted, orbital ripples dominate ripple types observed in laboratory studies, whereas anorbital ripples are the most commonly found type in field settings deep enough that the waves can reasonably be considered small amplitude. This is a consequence of the fact that orbital ripples are generally found at smaller wave orbital diameters than are anorbital ripples, and, largely owing to differences in period, the orbital diameter of oscillatory flows in wave tanks and tunnels is generally significantly lower than that typically found on the continental shelf. Thus the difference in ripple type in the two environments appears to be largely a result of the lack of substantial overlap in wave period in field and flume settings.

The proportionality between the wavelength of orbital ripples and the orbital diameter of the accompanying oscillatory flow suggests that wave motion, probably coupled with the lee vortices forming on both sides of each crest, directly controls ripple spacing for these bed forms. The velocity pattern measured by *Ikeda et al.* [1991], averaged over the period of oscillation, shows two stationary cells each occupying half the distance between crests and extending to several times the ripple height. Once orbital ripples are established, it appears that they persist as long as sediment is predominantly being transported as bed load. If shear velocity is increased without commensurate increases in the period of oscillation, the wave boundary layer will increase in thickness. At the same time, the flow conditions will approach those necessary to begin moving some of the sediment in suspension, particularly sediment near the crest where the local shear stresses are highest. As the ripples lose sediment at their crests to suspension, their heights decrease and, eventually, the ratio of wave boundary layer thickness to ripple height will increase to the point where the ripples are completely submerged in the wave boundary layer. Some of the available data sets that include measurements spanning this transition [e.g., *Inman*, 1957; *Carstens et al.*, 1969; *Mogridge and Kamphuis*, 1972] suggest that this transition is accompanied by an adjustment in ripple wavelength such that two or more ripples fill the space originally occupied by one, until a new spacing of the order of 500-600D is established. At the same time, however, the sediment forming the ripples continues to go into suspension, so that the bed is also approaching upper plane bed conditions as shear velocity is increased.

The *Southard et al.* [1990] flume measurements appear to provide an exception to this generalization, in that large-scale oscillatory bed forms with wavelengths roughly consistent with orbital ripple scales (i.e., $\lambda_{orb} \approx 0.62 d_o$) are observed under suspended-sediment transporting conditions. Superimposed on these are smaller-scale ripples with spacings that suggest they are anorbital ripples. The crests of the larger forms are rounded. As a result, lee vortices, if they exist at all, are unlikely to have scales approaching half the wavelength of the bed forms, suggesting the scale of the vortices is not the primary control on spacing of orbital ripples. A cross-sectional view of the stratification associated with the large-scale oscillatory bed forms shows similarities with some types of hummocky cross-bedding observed in ancient shallow marine deposits [*Southard et al.*, 1990]. If our hypothesis is correct that the large-scale bed forms in the *Southard et al.* [1990] experiments are essentially orbital ripples that form under conditions when a significant amount of sediment is moving in suspension, but the suspended load is largely confined to a thin, high concentration layer, then it may be possible using some of the methods described herein to constrain the possible surface wave conditions that could produce this type of bed form. As *Southard et al.* [1990] also note, the flow would have to be nearly purely oscillatory. Any significant superimposed current would allow suspended sediment to diffuse out of the wave boundary layer reducing the likelihood that there would be sufficient deposition during the required high oscillatory flows to produce a bed form with an appreciable height.

The spacing of 500-600D for anorbital ripples in our primary data set is similar to the spacings observed for unidirectional current ripples. *Yalin* [1977], for example, suggests that ripple spacing in steady flows is of the order of 1000D. This suggests that the instability mechanism governing the wavelength of anorbital ripples may be related to that controlling ripple wavelength in steady flows. Because the orbital diameter is much larger than ripple spacing for anorbital ripples, from the standpoint of sediment transport the flow might be considered quasi-steady over part of the wave cycle. An important feature of natural wave settings, such as the continental shelf, is that the bed is continually subjected to wave forcing over long periods of time. Ripples tend to persist until a large wave event suspends enough of the bed material that the preexisting ripples are washed out and upper plane bed conditions are established. As wave height and the wave-generated shear stresses decrease back to normal levels, suspended sediment will return to the bed and bed load will once again dominate the transport. As this occurs, ripples will quickly reform.

These observations point toward another important difference between ripples found in flumes and in the field, namely, that in flumes ripples are usually first formed under lower plane bed conditions and continue to develop as orbital diameter is increased, whereas in the field ripples are more likely to form as orbital

diameter decreases following upper plane-bed (sheetflow) conditions. Other differences that are likely to contribute to the greater variability of anorbital ripple spacing compared to orbital ripples is that, whereas the oscillations in flumes tend to be simple sinusoidal motions and the bed material is relatively well sorted, the wave field impinging on the continental shelf is characterized by a range of wave heights and periods, there is often a superimposed current, and the bed material in natural settings is generally more heterogeneous. Our analysis of field ripples utilizes significant wave height except for the *Miller and Komar* [1980b] data in which the several discrete frequencies containing significant energy were used. Laboratory measurements simulating field wave conditions are probably necessary to gain further insight into the characteristics of ripples formed by a complex wave field. We have neglected any effects of superimposed currents. Consequently, our approach is best suited to environments in which the bed shear stress is dominated by the contribution of waves, as is commonly the case on the inner to mid-continental shelf. However, inasmuch as wave-formed anorbital ripples have wavelengths similar to current-formed ripples, estimates of ripple scales using our method may provide a reasonable approximation even for cases where currents dominate, although the ripples would be expected to have more asymmetric shapes under current-dominated conditions.

If our assessment of orbital ripples is correct, that is, if orbital ripple height is significantly greater than wave boundary layer thickness, there are implications for the methods generally used to calculate wave-generated shear stresses. Because the dominant roughness elements, i.e., the ripples, are larger than the boundary layer, the unsteady boundary layer theory used to compute wave friction factor and the values of u_{*m}/u_{om} plotted in Figure 6 can not be expected to apply. This includes the algorithms currently used for computing wave shear stress in wave-current boundary layer models. Fortunately, the ripples found most commonly in field settings are anorbital or suborbital, and these can generally be analyzed with the usual methods. The complication for anorbital ripples is that the computed stress is not the shear stress at the bed surface, so a form-drag correction of some sort is necessary. Regardless of ripple type, accelerations in time and space of an oscillatory flow over a rippled bed result in spatial and temporal variations in bed shear stress, the effect of which on transport can only be approximated by representing bed shear stress as a single, characteristic value.

CONCLUSIONS

The large set of field and laboratory measurements of ripples formed under oscillatory flows compiled in this study supports the hypothesis that there are two primary ripple types, orbital ripples with spacings controlled by wave orbital diameter, and anorbital ripples with spacings governed by the grain size of the bed sediment. Suborbital ripples are intermediate forms. Our analysis of these measurements indicates that the parameter that best explains the differences between the primary ripple types is the ratio of wave boundary layer thickness to ripple height, or its close counterpart, the ratio of near-bed wave orbital diameter to ripple height. With this discriminator, and the simplest possible relationships describing the observed wavelength and steepness of orbital and anorbital ripples, we have constructed a method for predicting ripple wavelength and height that is simple and relatively accurate. It avoids the distinctions between field and flume cases made by *Nielsen* [1981] and provides substantially better estimates of anorbital ripple wavelength and height than does the *Grant and Madsen* [1982] method.

The relationship between wave boundary layer thickness and ripple height provides a plausible physical explanation for the differences in observed ripple types, but many questions remain unanswered. Among these are the instability mechanism governing the spacing of orbital and anorbital ripples, the proper method for computing the boundary shear stress on ripples under oscillatory flows when the ripple roughness length exceeds wave boundary layer thickness, the appropriate representation of a complex wave field, and the correct way to compute skin friction on bed forms submerged in the boundary layer. Many of the concepts and calculations described here can be applied to the interpretation of wave-formed structures in shallow marine deposits. This raises another set of questions but also offers the possibility of providing some quantitative constraints on wave conditions at the time of deposition.

Acknowledgments. This work was supported by the Office of Naval Research under grant N00014-90-J-1079 and N00014-91-J-1349. We thank Jody Bourgeois for providing information about the Elkton deposit and permitting us to use her drawing (Figure 13) and J. D. Smith for insightful discussions in the early stages of this work. We also appreciate the comments made by D. E. Drake, D. A. Cacchione, S. R. McLean, and C. Jette on an earlier draft of the paper.

REFERENCES

Bagnold, R. A., Motions of waves in shallow water; interaction between waves and sand bottoms, *Proc. R. Soc. London, Ser. A, 187*, 1-15, 1946.

Cacchione, D. A., and D. E. Drake, A new instrument system to investigate sediment dynamics on continental shelves, *Mar. Geol., 30*, 299-312, 1979.

Cacchione, D. A., D. E. Drake, W. D. Grant, and G. B. Tate, Rippled scour depressions on the inner continental shelf off central California, *J. Sediment. Petrol., 54*, 1280-1291, 1984.

Cacchione, D. A., M. E. Field, D. E. Drake, and G. B. Tate, Crescentic dunes on the inner continental shelf off northern California, *Geology, 15*, 1134-1137, 1987.

Carstens, M. R., F. M. Neilson, and H. D. Altinbilek, Bed forms generated in the laboratory under an oscillatory flow: analytical and experimental study, *Tech. Memo 28*, 39 pp., U. S. Corps of Eng., Coastal Eng. Res. Cent., Washington, D. C., 1969.

Clifton, H. E., Wave-formed sedimentary structures: A conceptual model, in Beach and Nearshore Sedimentation, edited by R. A. Davis, Jr. and R. L. Ethington, *SEPM Spec. Publ., 24*, 126-148, 1976.

Clifton, H. E., and J. R. Dingler, Wave-formed structures and paleoenvironmental reconstruction, *Mar. Geol., 60*, 165-198, 1984.

Dingler, J. R., Wave-formed ripples in nearshore sands, Ph.D. thesis, 136 pp., University of Calif., San Diego, 1974.

Dott, R. H., and K. J. Bird, Sand transport through channels across an Eocene shelf and slope in southwestern Oregon, U.S.A., in Geology of Continental Slopes, *SEPM Spec. Publ., 27*, 327-342, 1979.

Drake, D. E., D. A. Cacchione, and W. D. Grant, Shear stress and bed roughness estimates for combined wave and current flows over a rippled bed, *J. Geophys. Res., 97*, 2319-2326, 1992.

Einstein, H. A., The bed-load function for sediment transport in open channel flows, *Tech. Bull. 1026*, pp. 1-71, U. S. Dept. of Agric. Soil Conserv. Serv., Washington, D. C., 1950.

Grant, W. D., and O. S. Madsen, Combined wave and current interaction with a rough bottom, *J. Geophys. Res., 84*, 1797-1808, 1979.

Grant, W. D., and O. S. Madsen, Movable bed roughness in unsteady oscillatory flow, *J. Geophys. Res., 87*, 469-481, 1982.

Horikawa, K., and A. Watanabe, A study on sand movement due to wave action, *Coastal Eng. Jpn., 10*, 39-57, 1967.

Ikeda, S., K. Horikawa, and K. Noguchi, Oscillatory boundary layer over a sand ripple model, *Coastal Eng. Jpn., 34*, 15-29, 1991.

Inman, D. L., Wave generated ripples in nearshore sands, *Tech. Memo. 100*, 66 pp., U. S. Army Corps of Eng., Beach Erosion Board, Washington, D. C., 1957.

Jensen, B. L., B. M. Sumer, and J. Fredsoe, Turbulent oscillatory boundary layers at high Reynolds numbers, *J. Fluid Mech., 206*, 265-297, 1989.

Jonsson, I. G., Measurements in the turbulent wave boundary layer, paper presented at 10th Congress, Int. Assoc. for Hydraul. Res., London, 1963.

Jonsson, I. G., Wave boundary layers and friction factors, *Coastal Engineering*, Proc. 10th Conf., Tokyo, 1966, vol. 1, 127-146, Am. Soc. Civil Eng., New York, 1967.

Kajiura, K., A model of the bottom boundary layer in water waves, *Bull. Earthquake Res. Inst., Univ. Tokyo, 46*, 75-123, 1968.

Kennedy, J. F. and M. Falcon, Wave generated sediment ripples, *Rep. 86*, Mass. Inst. of Technol. Hydrodyn. Lab., Cambridge, 1965.

Long, C. E., A simple model for time-dependent stably stratified turbulent boundary layers, *Spec. Rep. 95*, Univ. of Wash., Seattle, 1981.

Manohar, M., Mechanics of bottom sediment movement due to wave action, *Tech. Memo. 75*, 121 pp., U.S. Army Corps of Eng., Beach Erosion Board, Washington, D. C., 1955.

Miller, M. C., and P. D. Komar, Oscillation sand ripples generated by laboratory apparatus, *J. Sediment. Petrol., 50*, 173-182, 1980a.

Miller, M. C., and P. D. Komar, A field investigation of the relationship between oscillation ripple spacing and the near-bottom water orbital motions, *J. Sediment. Petrol., 50*, 183-191, 1980b.

Mogridge, G. R., and J. W. Kamphuis, Experiments on bedform generation by wave action, *Coastal Engineering*, Proc. 13th Conf., Vancouver, B. C., 1123-1142, Am. Soc. Civil Eng., New York, 1972.

Nielsen, P., Dynamics and geometry of wave-generated ripples, *J. Geophys. Res., 86*, 6467-6472, 1981.

Schlichting, H., *Boundary Layer Theory*, 7th ed., pp. 615-623, McGraw-Hill, New York, 1979.

Smith, J. D., Modeling of sediment transport in continental shelves, in *The Sea, vol. 6*, edited by E. D. Goldberg, pp. 539-577, Wiley-Interscience, New York, 1977.

Smith, J. D., and S. R. McLean, Spatially averaged flow over a wavy surface, *J. Geophys. Res., 82*, 1735-1746, 1977.

Southard, J. B., J. M. Lambie, D. C. Federico, H. T. Pile, and C. R. Wiedman, Experiments on bed configurations in fine sands under bidirectional purely oscillatory flow, and the origin of hummocky cross-stratification, *J. Sediment. Petrol., 60*, 1-17, 1990.

Trowbridge, J., and O. S. Madsen, Turbulent wave boundary layers, 1, Model formulation and first-order theory, *J. Geophys. Res., 89*, 7989-7997, 1984.

Vongvisessomjai, S., Oscillatory ripple geometry, *J. Hydraul. Eng., 110*, 247-266, 1984.

Wiberg, P. L., and D. M. Rubin, Bed roughness produced by saltating grains, *J. Geophys. Res., 94*, 5011-5016, 1989.

Wiberg, P. L., and J. M. Nelson, Unidirectional flow over asymmetric and symmetric ripples. *J. Geophys. Res., 97*, 12745-12761, 1992.

Yalin, M. S., *Mechanics of Sediment Transport, 2nd ed.*, p. 247, Pergamon, New York, 1977.

Yalin, M. S., and R. C. H. Russell, Similarity in sediment transport due to waves, *Coastal Engineering*, Proc. 8th Conf., Mexico City, 1962, 151-167, Council on Wave Research, Richmond, California, 1963.

C. K. Harris and P. L. Wiberg, Department of Environmental Sciences, Clark Hall, University of Virginia, Charlottesville, VA 22903.

(Received December 7, 1992; revised August 27, 1993; accepted August 30, 1993.)